Chinese Chemical Letters 37 (2026) 112516

Contents lists available at ScienceDirect

Chinese Chemical Letters

journal homepage: www.elsevier.com/locate/cclet

Single-atom based graphdiyne catalysts support for CO_2 photo/electro-conversion

Fangzhou Yang[a,b], Yangmin Ma[a,*], Siyue Ma[a], Linli Xu[b,*]

[a] Key Laboratory of Chemical Additives for China National Light Industry, College of Chemistry and Chemical Engineering, Shaanxi University of Science & Technology, Xi'an 710021, China

[b] Department of Applied Biology and Chemical Technology and Research Institute for Smart Energy, The Hong Kong Polytechnic University, Hong Kong, China

ARTICLE INFO

Article history:
Received 23 May 2025
Revised 12 January 2026
Accepted 10 February 2026
Available online 10 February 2026

Keywords:
Single atom-based catalysts (SACs)
Graphdiyne (GDY)
CO_2 reduction reaction (CO_2RR)
Photo/electro-conversion

ABSTRACT

Climate change and global warming constitute formidable global challenges, predominantly driven by the excessive dependence on conventional fossil fuels, which results in substantial carbon dioxide (CO_2) emissions. Addressing these environmental issues is a paramount priority for researchers. Single-atom catalysts (SACs) have attracted significant attention due to their high atomic efficiency and unique performance in various catalytic reactions. As an emerging two-dimensional (2D) carbon material, graphdiyne (GDY) has gained favor in environmental remediation applications in recent years. GDY comprises sp- and sp^2-hybridized carbon atoms, which form benzene rings and diacetylenic linkages (–C≡C–C≡C–) within a two-dimensional planar network, endowing it with high π-conjugation, distinctive and tunable electronic properties, and excellent chemical and thermal stability. In this review, we investigate the environmental catalytic reactions and applications of GDY-based SACs. We provide a detailed account of the current methodologies for synthesizing GDY and examine the catalytic applications of GDY-based SACs in CO_2 reduction reactions. Specifically, we systematically categorize the photocatalytic and electrocatalytic CO_2 reduction processes using metal-doped GDY and metal-free doped GDY. Finally, we discuss the challenges and future developments of GDY within the context of SACs.

© 2026 Published by Elsevier B.V. on behalf of Chinese Chemical Society and Institute of Materia Medica, Chinese Academy of Medical Sciences.

1. Introduction

The atmospheric concentration of carbon dioxide (CO_2) has risen to levels unprecedented in the historical record, now exceeding pre-industrial values by more than 50%. This substantial increase is primarily ascribed to anthropogenic activities, notably the combustion of fossil fuels, large-scale deforestation, and various industrial processes [1–3]. The ramifications of elevated CO_2 concentrations are extensive, encompassing global climate destabilization, an increased frequency and intensity of extreme weather phenomena, and the acceleration of sea level rise, among other effects. The catalytic conversion of excess atmospheric CO_2 into value-added fuels and chemicals *via* photocatalytic processes represents a promising strategy, simultaneously contributing to the reduction of greenhouse gas emissions and addressing the challenges associated with renewable energy storage [4–8]. Among the CO_2 reduction reaction (CO_2RR) configurations, photocatalytic and electrocatalytic reactions are crucial strategies for CO_2 reduction and energy storage. However, there are many shortcomings in conventional catalysis, such as the low utilization rate of atoms, unclear selection of active sites and poor selectivity of catalysis [5,9–11]. Consequently, many efforts have been devoted to overcoming the deficiencies of traditional catalysts by efficiently developing new atomic-site catalysts.

Single-atom catalysts (SACs) have emerged as a novel class of heterogeneous catalysts, characterized by single atoms serving as the catalytic active centers [12–14]. They have garnered significant attention due to their optimal metal/free metal utilization and uniformity in active site composition [15–18]. In SACs, the electronic structure of isolated metal centers significantly impacts the adsorption energy of reactants and intermediates [11,19,20]. the atomically dispersed atoms exhibit strong charge transfer interactions with the substrate, facilitating the regulation of the coordination environment of active sites [21–23]. Moreover, SACs with homogeneous metal centers facilitate the study of catalytic mechanisms. SACs based on both precious and non-precious metals is crucial for advancing catalysts for sustainable applications, despite the inherent challenges involved.

Graphdiyne (GDY), in virtue of the unique electronic structure of carbon-carbon triple bond, it has recently been used as an excel-

* Corresponding authors.
E-mail addresses: mayangmin@sust.edu.cn (Y. Ma), linli.xu@polyu.edu.hk (L. Xu).

https://doi.org/10.1016/j.cclet.2026.112516
1001-8417/© 2026 Published by Elsevier B.V. on behalf of Chinese Chemical Society and Institute of Materia Medica, Chinese Academy of Medical Sciences.

lent platform for the incorporation of several metals or non-metals to fabricate SACs [24,25]. Li *et al.* successfully synthesized large-area GDY films *via* a cross-coupling reaction on copper surface for the first time, making a significant advancement. The unique arrangement of carbon atoms in GDY imparts it with remarkable physicochemical properties, including diverse chemical bonds, a highly ordered π-conjugated structure, abundant natural pores, an intrinsic band gap, high charge mobility, excellent electronic conductivity, and strong stability [26–32]. Despite these attributes, the pristine GDY is not inherently suitable for direct photo/electrocatalysis [33–35]. However, the photo/electro-catalytic activity can be enhanced through heteroatom doping [36]. Additionally, GDY is a leading candidate among carbon-based materials for supporting atomic catalysts [37]. The discovery and synthesis of GDY have significantly advanced the application of SACs, enhancing reaction efficiency [38]. The unique triangular pores and rich carbon skeleton of GDY are instrumental in capturing and stabilizing single atoms. Uniformly anchoring these catalytically active single atoms on two-dimensional GDY effectively increases the active area of the catalysts [39–45]. Compared to conventional two-dimensional carbon supports such as graphene and graphitic carbon nitride (g-C_3N_4), GDY offers distinct advantages for stabilizing SACs. The unique structure of GDY, featuring alternating benzene rings and diacetylene linkages, creates abundant intrinsic pores and a highly π-conjugated framework. These characteristics provide numerous coordination sites and strong chemical interactions for anchoring single atoms, effectively preventing their aggregation and migration. Additionally, the high chemical reactivity of GDY's diacetylene bonds enables robust bonding with metal atoms, further enhancing the stability and dispersion of SACs. In contrast, graphene lacks sufficient anchoring sites, and g-C_3N_4 suffers from limited conductivity and structural stability. Thus, GDY serves as an ideal platform for the efficient stabilization of SACs, quantitative comparisons of atomic utilization efficiency and charge transfer kinetics would strengthen, surpassing other 2D carbon materials in this regard. This configuration markedly enhances the photo/electrocatalytic activity of GDY monoatomic catalysts compared to conventional catalysts [9,46]. Investigating the coordination engineering of GDY-based ACs could significantly advance their catalytic applications.

Herein, this review primarily examines the recent advancements in GDY-based atomic catalysts applied in CO_2RR. Initially, we explore the coordination environments of single metal and free metal atoms anchored on GDY, alongside their electronic structures and charge transfer characteristics. Subsequently, we discuss the progress and properties of GDY-based ACs in photocatalytic and electrocatalytic CO_2 reduction reactions, elucidating the underlying mechanisms. Finally, from the perspective of material preparation, we analyzed the current shortcomings and challenges to expand. From the perspective of industrial application, we gave suggestions in terms of process, economy, and environmental protection. Finally, in terms of catalytic application, we looked forward to the CO_2 catalytic application of single-atom doped GDY materials, especially the limitations and improvements of metal-anchored GDY. This will help the subsequent development and catalytic application of single-atom doped GDYs.

2. Structure of graphdiyne

As a novel carbon material, GDY with sp^2-/sp-hybridized carbon atoms exhibits unique structures and remarkable properties [41,47]. In GDY, adjacent benzene rings are interconnected by six diacetylenic bonds, creating an infinitely extending two-dimensional coplanar network [48]. The fundamental topological unit of GDY is a triangular pore composed of an 18-carbon ring [49–54]. The carbon bonds in GDY can be classified into four types: C(sp)–C(sp) triple bonds, C(sp)–C(sp) single bonds within diacetylene groups, C(sp^2)–C(sp^2) double bonds in benzene rings, and C(sp)–C(sp^2) single bonds that link benzene rings and diacetylene groups (Fig. 1) [49–54]. GDY features a highly π-conjugated configuration, with electrons extensively delocalized across its planar structure, which reduces the system's energy and provides significant chemical stability [55,56]. The two-dimensional planar layers of GDY are stacked through van der Waals forces and π-π interactions, and its distinctive electronic structure contributes to its high electrical conductivity [57].

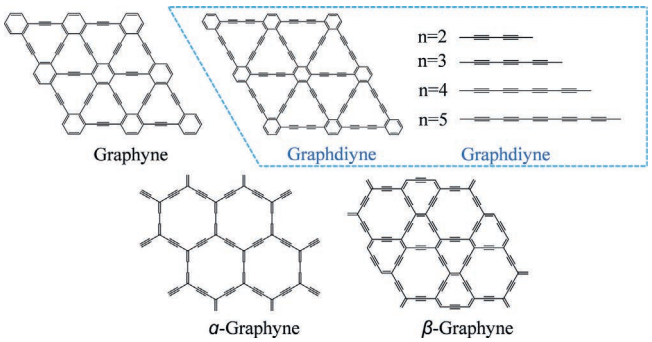


Fig. 1. The chemical structures of graphdiyne and other GYs.

Due to the numerous C–C bonds present in the structure of GDY, it exhibits high π conjugation, broad planar spacing, and uniformly distributed pores, which contribute to its desirable electrical conductivity and chemical stability. These properties facilitate the application of GDY in fields such as electronics, energy, photovoltaics, and catalysis [58]. Compared to conventional catalysts, GDY can markedly enhance the catalytic efficiency and durability of catalytic materials in redox reactions, electrocatalysis, photocatalysis. In contrast to graphene, the unique chemical structure of GDY can be tailored through the rational design of precursor molecules and coupling reaction pathways. The acetylene bonds in GDY can modulate the electronic properties of loaded single atoms, thereby enhancing catalytic activity. Additionally, a strong interaction exists between single atoms and GDY, ensuring their uniform distribution and preventing aggregation, which contributes to the long-term stability of electrocatalytic reactions. For electrocatalyst materials, GDY can effectively enhance catalytic stability due to its favorable conductivity and capacity, making it suitable for use as an energy storage material [59]. Furthermore, GDY has significantly influenced the field of carbonization, leading to numerous advancements in the environmental applications of carbon-based materials.

3. Synthesis of SACs graphydiyne

3.1. Synthesis of metal single-atom doped graphdiyne

3.1.1. Self-reduction and chemical-assisted reduction

Self-reduction and chemical-assisted reduction methods are direct and universal approaches for constructing atomically coordinated (AC) GDY. Cai *et al.* first synthesized Fe-GDY catalysts by adsorbing Fe^{3+} ions onto the GDY surface through vigorous stirring with $FeCl_3$. Both Fe-GDY and Cu-GDY with four-coordinate spheres were constructed by reducing aqueous GDY solutions containing Fe or Cu ions using $NaBH_4$ [60]. In a typical synthesis by Lu *et al.*, Pd-GDY was prepared by adding K_2PdCl_4 as a precursor into a GDY dispersion and stirring for 2 h. Using a different precursor $PdCl_2$ [61], Li *et al.* synthesized Pd/GDY ACs with distinct coordination spheres involving four palladium atoms. Additionally, Zhang *et al.* prepared a Pd-GDY/G heterojunction material utilizing both self-

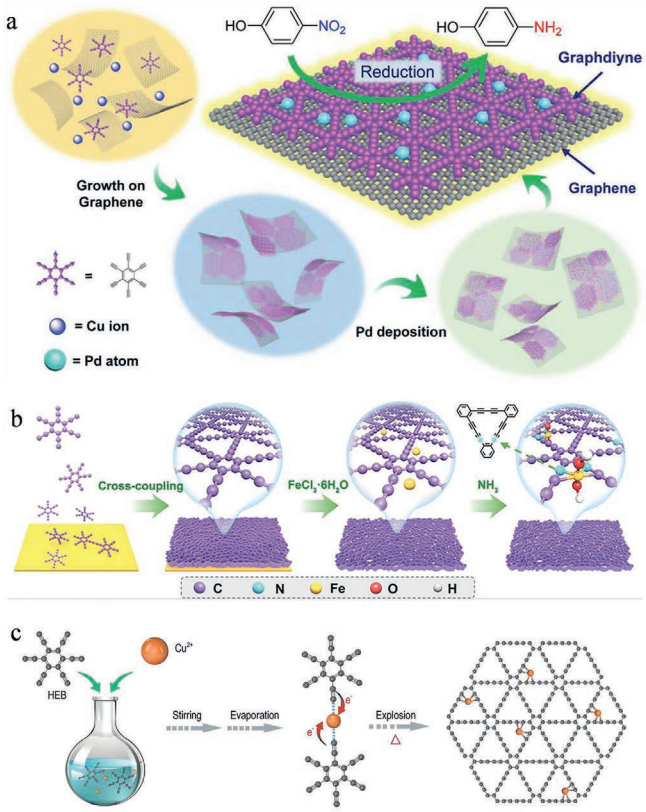


Fig. 2. Illustration of the synthesis procedures for (a) Pd/GDY/GD CAs. Reprinted with permission [62]. Copyright 2019, John Wiley and Sons. (b) Synthesis of the catalysts including Fe–GDY. Reprinted with permission [63]. Copyright 2022, John Wiley and Sons. (c) Cu/GDY. Reprinted with permission [64]. Copyright 2022, Oxford University Press.

reduction and $NaBH_4$ chemical reduction processes, as shown in Fig. 2a [62].

3.1.2. High-temperature treatment

Subsequently, high-temperature treatment techniques—including solvothermal synthesis, pyrolysis, and annealing—have emerged as versatile and effective strategies for the fabrication of atomically coordinated (AC) GDY materials. Huang *et al.* introduced a facile pyrolytic approach for anchoring iron (Fe) single atoms onto nitrogen-doped GDY, thereby establishing a six-fold coordination environment. In this method, GDY precursors pre-adsorbed with Fe^{3+} ions were subjected to calcination and pyrolysis under an ammonia atmosphere at 900 °C, resulting in the formation of novel Fe-N-GDY atomically coordinated structures (Fig. 2b) [63]. Li *et al.* successfully synthesized Cu_1/GDY by stirring $Cu(OAc)_2$ with GDY in solution, removing the solvent (Fig. 2c), and then transferring the resulting powder to a beaker for an ultra-fast reaction at 120 °C [64], and Li's group prepared Mo_n/GDY by dissolving Na_2MoO_4 in an argon-degassed aqueous solution, stirring for 5 h, and then transferring the solution into a Teflon-lined stainless-steel autoclave containing a piece of preprepared GDY at 120 °C [65].

Especially, the matrixes are usually prepared for the first and then the metal atoms are modified onto them by various methods. In 2020, Duan's group first reported the self-catalysis technique to achieve three GDY-based ACs, Rh-GDY, Co-GDY and Ru-GDY with four-coordinate M-C binding modes. And then, they used the same methods to prepared Cu-GDY materials with different sizes. Including single atoms and nanocluster by adjusting the amount of CuI in this system [66].

3.1.3. Electrochemical deposition

Finally, the electrochemical deposition method offers a rapid approach for preparing catalysts. Li's group successfully synthesized two GDY-based atomically coordinated structures, Ni-GDY and Fe-GDY, featuring four metal-carbon (M-C) bonds for the first time using electrochemical deposition. GDY was synthesized *in situ* on the surface of carbon cloth (CC) through a classical coupling synthesis method to form GDY/CC. This composite was then employed as the cathode for galvanostatic deposition in a dilute solution containing Ni^{2+} or Fe^{3+} ions to achieve the desired atomically coordinated structures [22].

3.2. Synthesis of metal-free single atom doped graphdiyne

3.2.1. High-temperature treatment

Huang *et al.* demonstrated that stable nitrogen-doped GDY (N-GDY) materials can be synthesized by treating GDY with ammonia at high temperatures, resulting in the uniform incorporation of nitrogen atoms [67]. X-ray photoelectron spectroscopy (XPS) confirmed the successful integration of nitrogen atoms into the GDY structure. Additionally, the potential nitrogen substitution sites in N-GDY were clearly illustrated. Compared to pristine GDY, the interlayer spacing in N-doped GDY slightly decreased, primarily due to the smaller atomic radius of nitrogen. Furthermore, it is anticipated that numerous heteroatom defects and active sites will be generated in N-doped GDY, significantly enhancing its performance. In a similar approach, Huang *et al.* intentionally doped pyridinic nitrogen into GDY by calcining it in an argon atmosphere after soaking it in a pyridine solution at room temperature. The N-doped GDY was further calcined in an ammonia atmosphere to increase the nitrogen doping level (Fig. 3a). The resulting catalysts exhibited desirable catalytic activity, along with improved stability and methanol tolerance compared to Pt/C [68–71]. Moreover, the doping of pyridinic nitrogen was theoretically shown to be an effective method for enhancing the catalytic activity of GDY. Other heteroatoms, such as boron (B) [72], sulfur (S) [71], phosphorus (P) [73], and fluorine (F) [74], have also been verified as beneficial for doping GDY, thereby improving its electronic structure and properties.

3.2.2. Heteroatom-incorporation

Furthermore, doping with various heteroatoms can effectively modulate the electrical and optical properties of GDY. Bu *et al.* reported the synthesis of boron (B) and nitrogen (N) co-doped GDY-based materials, which exhibited stable configurations and tunable band gap energies [2]. The study provided a detailed analysis of the doping process and examined the effects of impurity concentration on the structure and properties of the products. At low doping levels, BN units tend to replace sp-hybridized carbon atoms in the chains, forming linear BN atomic chains between carbon hexagons [37]. At higher doping levels, BN units initially replace sp-hybridized carbon atoms within the carbon hexagons, subsequently replacing the carbon atoms in the chains, which consist solely of sp^2-hybridized carbon atoms. Compared to graphene, the B/N doping process in GDY is more facile. Notably, the direct band gap characteristics of BN-doped GDY remain unchanged regardless of the doping concentration. Research conducted by Kang's group further demonstrated that co-doping with three elements B, N, and O, can significantly alter the electrical properties of GDY [39,75]. The specific doping sites of these elements play a critical role in modulating its electrical characteristics. In addition to the doping methods, there is an alternative approach where single atoms of B, P, and Si are used as ligands to directly synthesize GDY under the catalysis of copper (Fig. 3b) [76]. This bottom-up synthesis method uniformly incorporates non-metallic elements B, P, and Si into the GDY material.

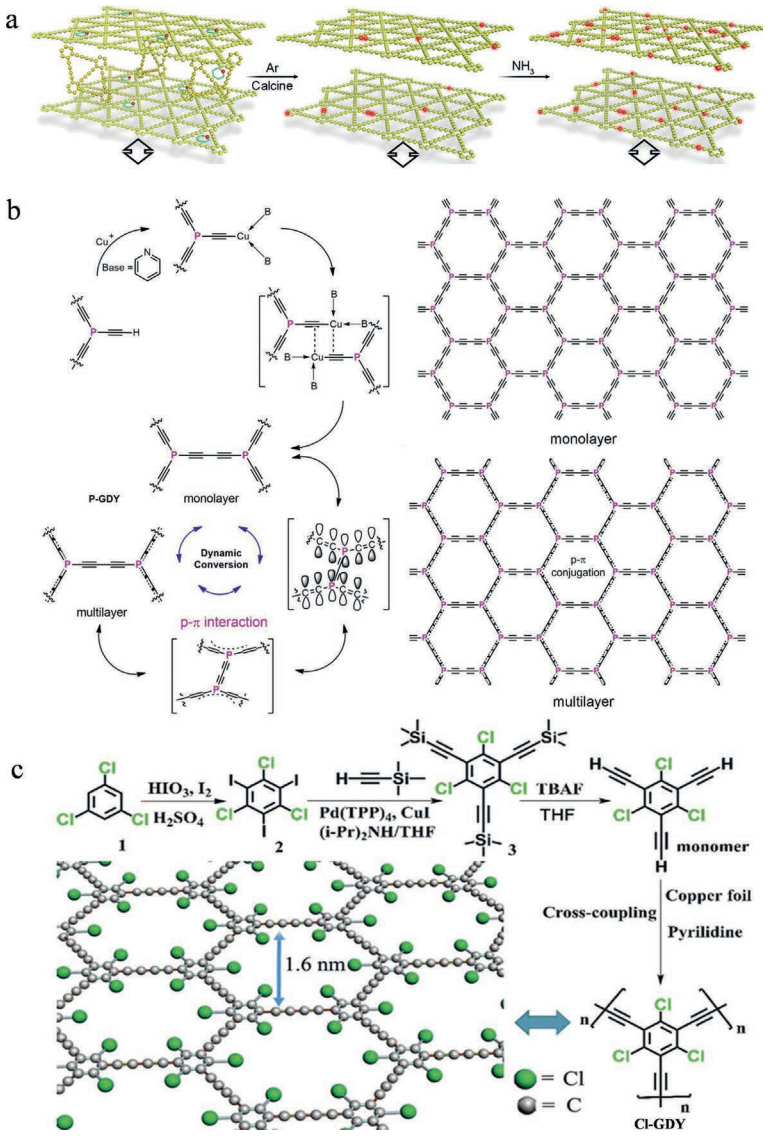


Fig. 3. (a) Synthesis and microstructure of the catalysts. Illustration of the N-doping process including Py−GDY, N-GDY-900 °C, and N′N-GDY. Reprinted with permission [67]. Copyright 2017, American Chemical Society. (b) Scheme of the synthetic process and structure for P-GDY, proposed mechanism for the preparation of P-GDY and structure of the monolayer P-GDY. Reprinted with permission [76]. Copyright 2023, American Chemical Society. (c) The structure and synthetic route to Cl-GDY. Reprinted with permission [77]. Copyright 2019, John Wiley and Sons.

3.2.3. "Bottom-up" strategies

Non-metallic elements such as nitrogen (N), phosphorus (P), and boron (B) have been incorporated into materials. The introduction of elements like fluorine (F), chlorine (Cl), bromine (Br), and iodine (I) is more straightforward and results in a more stable structural integration. This is because heteroatoms are directly bonded to ligands to form halogenated aromatics, leading to a more stable and uniform distribution within the material compared to post-synthesis doping of heteroatoms in GDY. However, achieving precise doping of heteroatoms using these top-down methods is challenging, as the amount and position of the doped heteroatoms cannot be accurately controlled. This limitation hinders further investigation into the effects of heteroatoms on the intrinsic properties of carbon materials. Therefore, there is an urgent need for a new, controllable doping/substitution strategy [74]. Drawing inspiration from the bottom-up approaches commonly employed in organic synthesis, it is possible to fabricate atomic-level doped GDY-based carbon materials with well-defined structures by utilizing specific monomers. For instance, hydrogen-substituted GDY (H-GDY), chlorine-substituted GDY (Cl-GDY) in Fig. 3c, and fluorine-substituted GDY (F-GDY) have been synthesized using triethynylbenzene [77], 1,3,5-triethynyl-2,4,6-trichlorobenzene, and 1,3,5-triethynyl-2,4,6-trifluorobenzene as monomers, respectively, through an *in situ* coupling reaction on copper foil [47,78]. In summary, the strong chemical tailor ability of alkynyl-containing monomers allows to produce a wide range of GDY derivatives with diverse chemical structures. By selecting appropriate monomers, it is possible to achieve the precise construction of specific heteroatom-doped GDY-based carbon materials.

4. CO_2 reduction reaction

In recent years, there has been a notable increase in atmospheric CO_2 levels, highlighting the urgent need to transform CO_2 into valuable and sustainable products [79–83]. Consequently, capturing, storing, and converting CO_2 have emerged as effective strategies for its mitigation. Among these, the CO_2RR primarily facilitates the conversion of CO_2 into useful chemicals, including

methane, methanol, and ethanol [84–89]. To enhance the versatility of the CO_2RR, various catalytic approaches such as thermal catalysis, biological catalysis, photocatalysis, and electrochemical catalysis have been explored. Given the inherent stability and sluggish reaction kinetics of CO_2, the development of highly active catalysts is essential. Extensive research has been conducted on various transition metals as potential CO_2RR catalysts. Currently, electrocatalysis and photocatalysis are regarded as promising green catalytic methods for advancing the CO_2RR [2,46,90–92].

4.1. Electrocatalytic CO_2RR by metal-SACs-GDY

The electrochemical CO_2RR offers a cost-effective and higher-yield alternative to conventional methods for converting CO_2 into carbon monoxide (CO), methane (CH_4), or complex hydrocarbon fuels [93–95]. Despite certain drawbacks, such as slow reaction kinetics, a variety of reduction products, low energy efficiency, limited catalyst stability, and competition from the hydrogen evolution reaction (HER), the electrocatalytic CO_2RR remains a promising technology for CO_2 utilization [96–102]. Identifying efficient catalysts is therefore crucial for advancing this process. SACs, with their distinctive structures and catalytic properties, hold significant potential for application in the CO_2RR [34,37,103,104]. Variations in the metal type or ligand environment can alter the electronic structure and properties of the metal center, enhancing catalytic performance [73,105–108]. SACs effectively bridge the gap between homogeneous and heterogeneous catalysts in the electrochemical CO_2RR. GDY also exhibits considerable electrocatalytic potential, contributing to CO_2 electrocatalysis [48,109–113]. By reducing noble metals to single atoms, SACs achieve superior catalytic performance compared to traditional metal nanoparticles [114–116]. Moreover, employing SACs is one of the most efficient strategies for reducing the cost associated with noble metals [117–121].

Transition metal silver holds significant potential in the electrocatalysis of the CO_2RR. Due to the unique electronic structure of GDY, it serves not only as a template for the growth of silver nanoparticles (AgNPs), effectively preventing their aggregation, but also enhances the conversion efficiency of active sites and electron transfer through strong interfacial interactions [122,123]. This synergy significantly boosts the electrocatalytic performance of the resulting nanocomposites. A novel CO_2RR catalyst, Ag/GDY/CC, was developed using a straightforward *in situ* synthesis method involving three steps based on GDY [25]. The intimate contact between components maximizes the exposure of the silver surface and effectively enhances charge transfer and electrocatalytic properties. The Ag/GDY/CC electrode shows a more positive onset potential (−0.2 V) than the other samples. Comparison of its linear scan voltammetry (LSV) curves in Ar- and CO_2-saturated solutions (Fig. 4a) further confirms its superior electrocatalytic activity. Experimental results demonstrated that the Ag/GDY nanocomposites achieve a Faradaic efficiency of 92.1 % for the electrochemical reduction of CO_2 to CO, with a high current density of 25.74 mA/cm^2, maintaining durability for up to 24 h (Figs. 4b and c). Throughout the catalytic process, Ag/GDY composites exhibit excellent stability. Compared to the X-ray photoelectron spectroscopy (XPS) patterns of pure GDY, the interaction between AgNPs and GDY shows more active electron interactions. Even after 2000 cycles, Ag/GDY/CC retains its electrochemical stability, as shown in Figs. 4d and e, making it a promising candidate for electrocatalytic CO_2RR (Fig. 4f). Silver-based electrocatalysts, known for their high catalytic activity, selectivity, and cost-effectiveness, have been extensively utilized in the field of catalysis. Among the three models, Ag (111)/GDY/CC exhibits the lowest free-energy barriers for both the formation of the COOH* and CO intermediates, as well as for the desorption of CO to gaseous CO. This indicates that Ag (111)/GDY/CC possesses superior electrocatalytic activity compared to GDY/Ag (111)/CC and Ag (111)/CC. The enhanced performance can be attributed to strong electronic interactions at the interface between GDY and Ag nanoparticles, resulting from the coupling of π/π orbitals in the sp^2-C and sp-C of GDY with the d orbitals of metallic silver. Consequently, the energy barriers for generating COOH and *CO intermediates on Ag (111)/GDY/CC are reduced by 0.3 eV compared to those on pure Ag particles, Figs. 4g and h demonstrate that Ag/GDY/CC exhibits the highest double-layer capacitance (12.75 mF/cm^2), 1.6 times that of Ag/CC and three times that of GDY/CC. Additionally, Ag/GDY/CC shows lower solution resistance ($R_s = 2.0\ \Omega$) and charge transfer resistance ($R_{ct} = 71.4\ \Omega$) than Ag/CC ($R_s = 3.0\ \Omega$, $R_{ct} = 158.6\ \Omega$) and GDY/CC ($R_s = 2.3\ \Omega$, $R_{ct} = 3180.1\ \Omega$), indicating superior electrochemical performance.

In recent years, the application of porous two-dimensional (2D) material coatings on metal surfaces has emerged as a promising strategy to enhance catalyst performance. Specifically, GDY coatings on copper (Cu) surfaces have paved a new avenue for electrocatalysis. Gas molecules can readily penetrate the interface between the 2D material and the metal, facilitating reactions within a confined "nano-reactor" beneath the 2D overlay. Density functional theory (DFT) calculations have highlighted the advantages of GDY coatings in lowering the free energy and onset potential of key intermediates. Peterson *et al.* demonstrated that Cu surfaces covered with GDY exhibit superior catalytic capabilities compared to conventional metal surfaces. The structures of CO_2 reduction intermediates on GDY-covered Cu surfaces were compared with those of key intermediates, COOH* and CHO*. It was observed that the binding of CO* surpasses that of the original transition metal. Electrochemical CO_2 reduction was more active beneath the GDY overlay (Figs. 5a and b) [90]. According to the DFT energy distribution along the pathway through the GDY triangular pores, CO_2 can easily traverse the GDY layer (Fig. 5c). GDY influences the relative free energy of CO_2 reduction on the Cu (111) surface and the relative free energy of each intermediate [124]. The incorporation of Cu enhances the activity for the CO_2 reduction reaction.

Although copper is widely regarded as the most efficient metal for the electrocatalytic reduction of CO_2, the initial voltage required for the reduction of CO_2 to hydrocarbons on a copper electrode is approximately 1 V [125,126]. The development of catalysts with higher activity is crucial for the practical implementation of CO_2 electrocatalytic reduction. Guo *et al.* demonstrated the advantages of two-dimensional confined catalysis by overlaying the copper surface with GDY, which, according to density functional theory calculations, reduces the free energies of key intermediates and the onset voltage. The theoretical analysis indicated that the electrochemical reduction of CO_2 beneath the GDY layer is enhanced due to the confinement effect. Furthermore, the energetic stabilization of reaction intermediates results in a lower onset voltage for CO_2 reduction to hydrocarbons on the GDY-coated copper surface compared to the pristine copper surface. This approach could serve as a straightforward and viable strategy for developing novel catalysts to improve CO_2 reduction performance by coating with GDY. SACs are particularly favored for their high catalytic activity [90]. Zhao *et al.* conducted the first theoretical investigation into the CO_2 electrocatalytic reduction performance of a monoatomic Fe/GDY catalyst. Their findings revealed that the Fe/GDY catalyst exhibits high stability, excellent electrical conductivity (Figs. 5d-f), and magnetic properties, which contribute to its superior performance in the electrocatalytic conversion of CO_2 into CH_4 and C_2H_5OH. The limiting potential (−0.43 V) is less negative than that of previously reported CO_2 electrocatalysts, such as cobalt porphyrin nanotubes (−0.56 V), Cu nanoparticles/graphene (−0.86 V) [127–130].

In addition to theoretical calculations, GDY-based electrocatalysts for CO_2RR have also demonstrated high efficiency in experimental studies [131]. The catalytic activity of bismuth sub carbon-

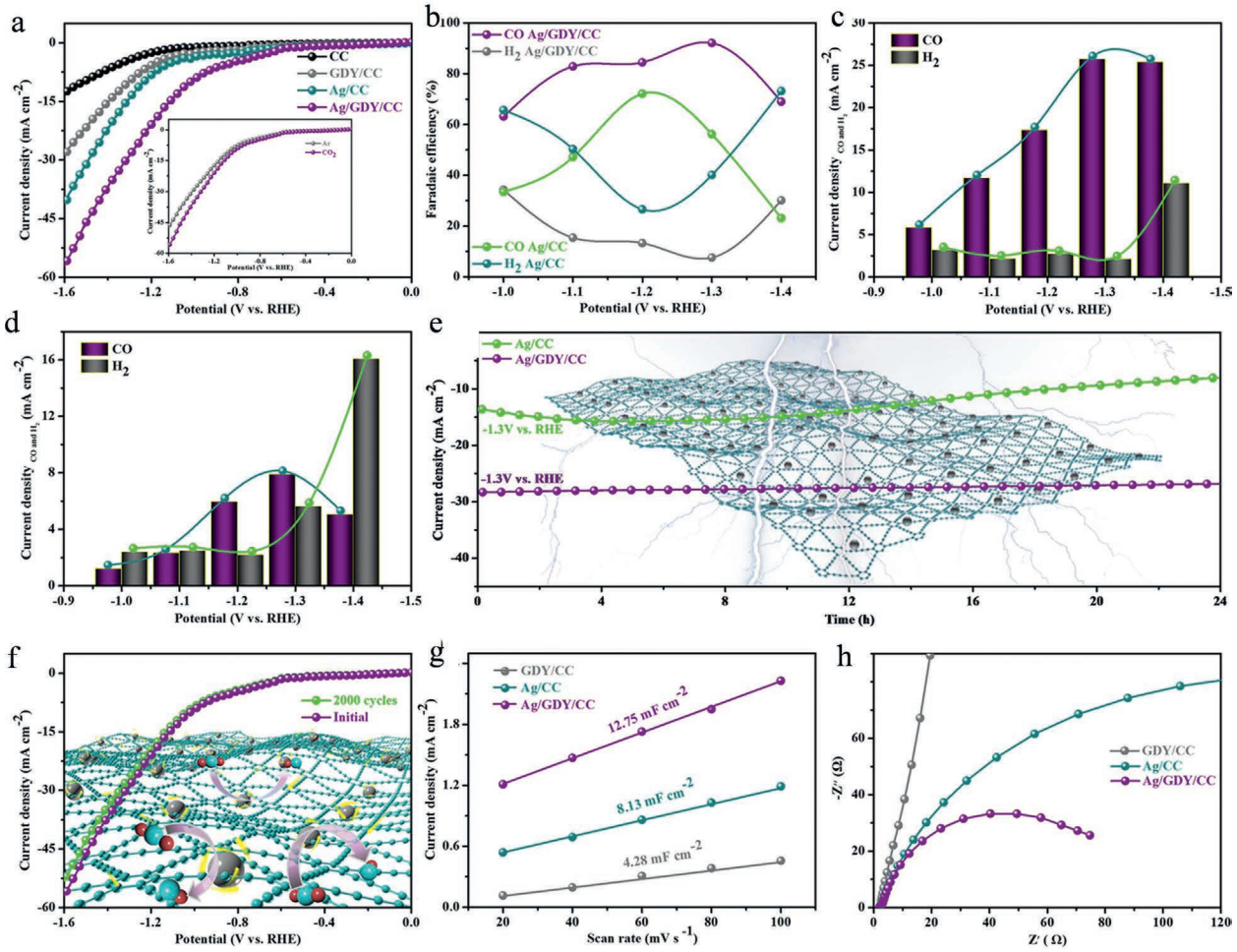


Fig. 4. (a) LSV curves. (b) Faraday efficiency of e-CO_2RR. CO and H_2 current density of (c) Ag/GDY/CC and (d) Ag/CC. (e) Current–time (*I*–*T*) curves of Ag/GDY/CC and Ag/CC. (f) Stability test of Ag/GDY/CC LSV curves. (g) Capacitive currents as a function of scan rates. (h) Electrochemical impedance spectroscopy of different samples. Reprinted with permission [25]. Copyright 2021, John Wiley and Sons.

Table 1
Single atom adsorption properties of main metals.

Catalyst	Faradaic efficiency (%)	Current density (mA/cm^2)	Product selectivity (%)	Ref.
Ag/GDY/CC	92.1	25.74	62	[25]
Ag/CC	72.1	7.89	22	[25]
Cu@GDY/Co	97	100	80	[32]
Cu SAs/GDY	66	24	97.6	[64]

ate was significantly enhanced following the introduction of a uniform GDY layer, which was attributed to the electron-rich acetylene bonds facilitating the reduction of Bi(III) to Bi(0) [18,89]. This promotional effect has been shown to extend to other metal electrocatalysts as well. Furthermore, the strong anchoring of GDY to active species and the resulting electronic interactions can significantly improve selectivity and stability by preventing molecular agglomeration. For instance, when ultrathin 2D GDY was employed as an adsorption layer to support cobalt phthalocyanine (CoPc) [32], the hybrid catalyst achieved a CO faradaic efficiency of 97% at a current density of 100 mA/cm^2. Several typical metal-anchored GDY are summarized and their performance tables are integrated (Table 1).

SACs loaded on GDY combined with electrochemical CO_2RR can significantly change the electronic properties and atomic structure of the central metal site of SACs by changing the type of SACs or the coordination environment due to the maximum theoretical atomic utilization and unique structure, providing an opportunity to design SACs for CO_2 electrocatalysis. In this case, the activity and selectivity of catalysts for the CO_2RR can be modulated at the atomic level. More attention should be paid to C–C coupling on SACs and the HER as a common side reaction of the CO_2RR. A combination of characterization methods and theoretical calculations should be used to further investigate the modulation of electrochemical CO_2RR by SACs loaded with GDY [132].

4.2. Photocatalytic CO_2RR by metal-SACs-GDY

Photocatalysis represents an ideal approach to reducing fossil fuel consumption and mitigating the greenhouse effect by converting CO_2 into chemical super fuels using cost-effective geothermal cooperative systems [44,87,111]. With the ongoing advancements in photocatalytic technology, solar-powered photocatalytic CO_2RR not only facilitate the production of high-energy fuels and high-value-added chemicals but also contribute to the reduction of CO_2 emissions [133–135]. This offers a promising strategy to tackle en-

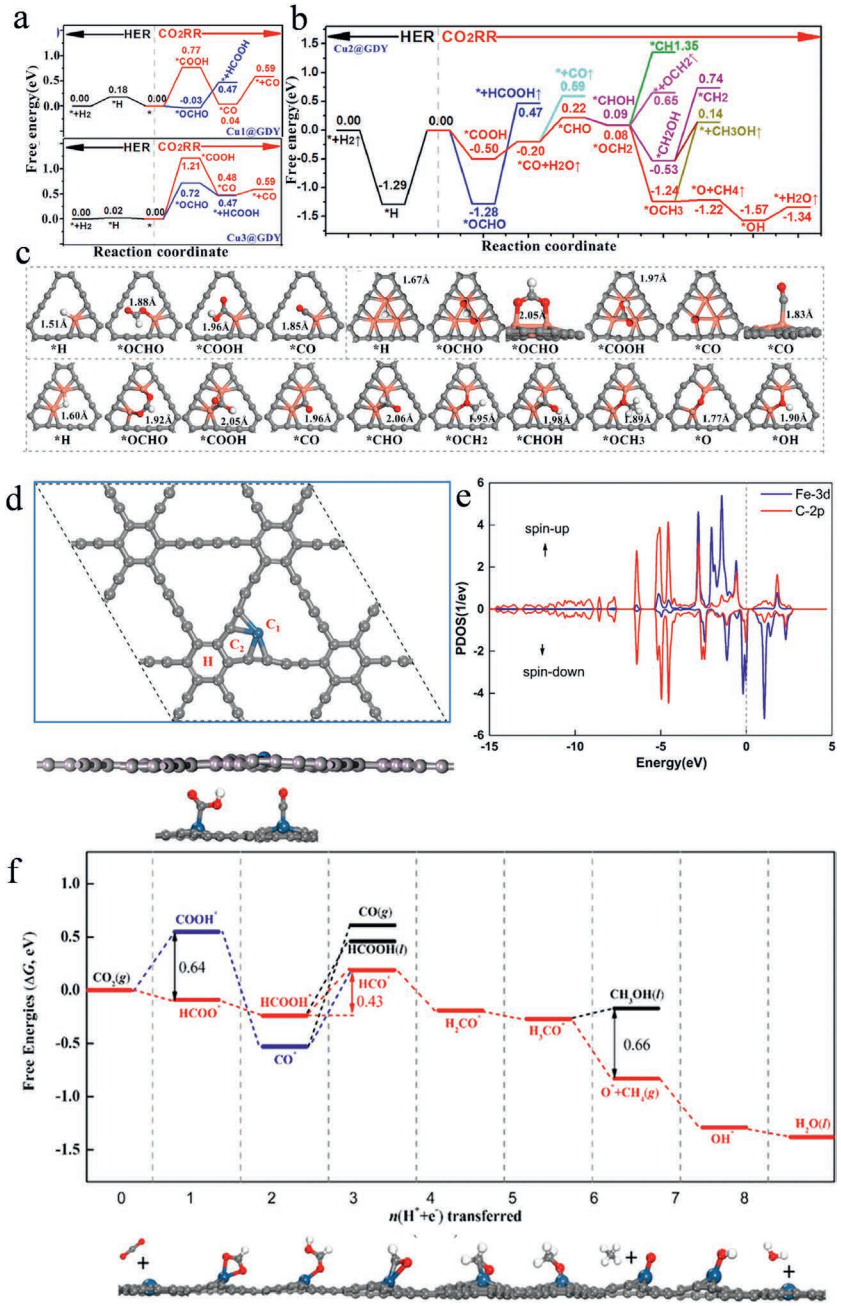


Fig. 5. (a, b) Free energy diagrams of CO_2RR. (c) HER and corresponding species on Cu1@GDY, Cu2@GDY, and Cu3@GDY surfaces. The gray, red, brown, and white balls represent C, O, Cu, and H atoms. Reprinted with permission [90]. Copyright 2020, Elsevier. (d) Optimized structure and (e) projected density of states of Fe/GDY. (f) Computed free-energy profile of the electrochemical reduction of CO_2 to CH_4 on Fe/GDY and the involved reaction intermediates. Reprinted with permission [129]. Copyright 2020, American Chemical Society.

ergy and environmental challenges. However, despite the development of numerous semiconductor photocatalysts, their effectiveness in CO_2 reduction is often limited by low conversion rates and selectivity [5,92,136–138]. Consequently, the development of efficient CO_2 photocatalysts remains a significant challenge in the field [40,78,139], metal SACs-GDY is the selectivity catalysts in this system.

A GDY film coating was applied to $CsPbBr_3$ nanocrystals to create a $CsPbBr_3$@GDY composite photocatalyst. The photocatalytic redox reaction was subsequently investigated, revealing that the catalyst doped with cobalt (Co) ions exhibited activity nearly eight times greater than that of pure $CsPbBr_3$, due to the high metal loading. The active sites provided by the doped Co ions and the enhanced chemisorption of CO_2 on GDY were key factors in the improved photocatalytic reduction of CO_2 to CO. The GDY coating facilitated the aggregation of CO_2 on the surface, and the presence of cobalt significantly increased the CO_2 adsorption capacity, further promoting photocatalysis. The XPS C 1s spectrum of $CsPbBr_3$@$GDY_{0.3}$ revealed six peaks, with the calculated integral ratio of sp- and sp^2-carbon close to 2, confirming the successful coating of GDY on the $CsPbBr_3$ nanocrystals. This approach offers a promising method for enhancing the performance of metal halide perovskite nanocrystals [140]. The encapsulation of $CsPbBr_3$ with a GDY layer effectively suppresses electron hole recombination [107], while the incorporation of Co^{2+} sites enhance the chemical adsorption of CO_2 on GDY (Figs. 6a-c), Photocurrent experiments show

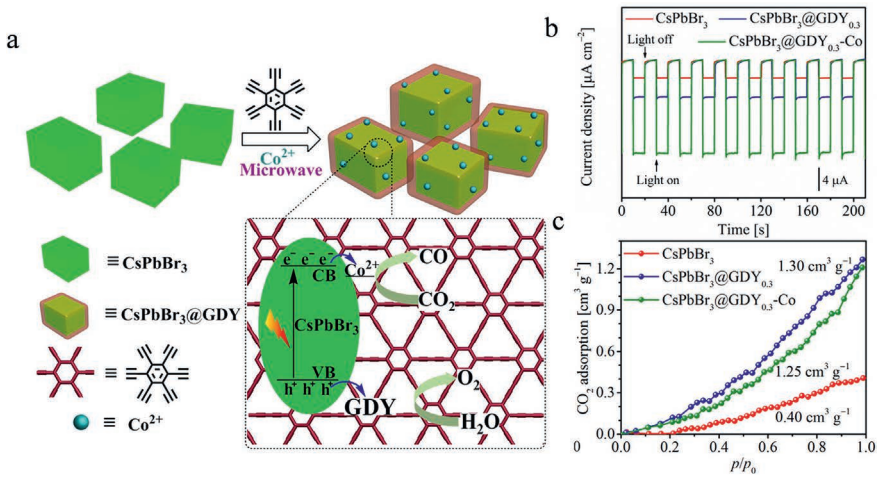


Fig. 6. (a) Schematic representation of photo redox reactions of cobalt doped $CsPbBr_3$@GDY. (b) *I*–*t* curves of $CsPbBr_3$, $CsPbBr_3$@$GDY_{0.3}$, and $CsPbBr_3$@$GDY_{0.3}$Co under light irradiation. (c) The adsorption curves of CO_2 for $CsPbBr_3$, $CsPbBr_3$@$GDY_{0.3}$, and $CsPbBr_3$@$GDY_{0.3}$Co. Reprinted with permission [107]. Copyright 2020, American Chemical Society.

that the charge separation efficiency of the doped material is improved (Fig. 6b). These factors are crucial for the improved photocatalytic reduction of CO_2.

Additionally, Yu *et al.* reported the synthesis of a GDY-decorated Ti heterojunction *via* electrostatic-driven self-assembly of Ti nanofibers and GDY nanosheets, specifically for photocatalytic CO_2 reduction. Compared to pristine TiO_2, the Ti/GDY catalysts demonstrated several advantages in photocatalytic CO_2 reduction. Notably, the delocalized electrons in GDY can hybridize with the vacant Ti 3d orbitals in TiO_2, facilitating the formation of an internal electric field at the interfaces and enhancing charge carrier separation upon photoexcitation. Furthermore, GDY strongly adsorbs and activates CO_2 molecules, as confirmed by density functional theory (DFT) calculations and *in situ* diffuse reflectance infrared Fourier transform spectroscopy. Importantly, the photothermal effect of GDY further enhances CO_2 adsorption, promoting subsequent photoreduction reactions. Indeed, the Ti/GDY composite with 0.5 wt% GDY exhibited superior reduction efficiency compared to pure TiO_2 [24]. Yu *et al.* also demonstrated that GDY, as a cocatalyst for photocatalytic CO_2 reduction, outperforms graphene. They successfully synthesized Cd on the GDY surface under solvothermal conditions with dimethyl sulfoxide. Theoretical calculations and experimental characterizations revealed that strong chemical bond interactions between GDY and Cd, along with the resultant sulfur vacancies and electron-deficient diacetylene bonds in the Cd^{2+}/GDY heterojunction, enhance electron transfer and create additional CO_2 adsorption sites. Consequently, the Cd^{2+}/GDY hybrid material exhibits superior efficiency in gas phase photocatalysis without requiring any sacrificial agents. Compared to the Cd^{2+}/graphene photocatalyst, the Cd^{2+}/GDY photocatalyst demonstrates higher activity, stability, and selectivity [97]. These findings confirm that GDY serves as a highly effective cocatalyst for enhancing the photoreduction activity of CO_2.

4.3. Electrocatalytic CO_2RR by metal-free ACs GDY

Metal-free catalysts are garnering increasing attention due to their advantages over conventional metal catalysts, such as reduced cost, enhanced selectivity, improved durability, and environmental friendliness. Recently, a novel class of carbon-based metal-free catalysts has demonstrated efficient catalytic performance [39,70]. However, the advancement of traditional carbon-based metal-free catalysts is still impeded by several challenges, including harsh synthesis conditions, limited intrinsic activity, poorly defined active sites, and unclear catalytic mechanisms [11]. GDY, with its highly inhomogeneous surface charge distribution, exhibits significant intrinsic catalytic activity. Furthermore, the structure and properties of GDY can be easily and precisely tailored through chemical modification, enabling the development of metal-free catalysts with well-defined structures and catalytic mechanisms [67,141].

Given the limited reserves of metals, scientists are committed to exploring high-performance metal-free catalysts based on carbon materials to address environment-related challenges. Doping can induce inhomogeneous charge distribution on the surface, which is an effective strategy for enhancing catalytic performance. Liu *et al.* have leveraged the unique sp-C in GDY to introduce a novel N doping configuration of sp-hybridized nitrogen (sp-N), which exhibits catalytic activity in the oxygen reduction reaction comparable to that of platinum [141]. eGDY-Click-700 demonstrates exceptional selectivity for CH_4 production from CO_2 electroreduction, achieving a CH_4/CO molar ratio of 3.4 in a 50:50 EMIM-BF_4:H_2O electrolyte at -0.60 V (*vs.* Ag/AgCl). In contrast, pristine eGDY is catalytically inactive for CO_2 reduction, generating only H_2 (Figs. 7a and b). The product selectivity is governed by the N-doping configuration: NH_3-doped eGDY favors CO ($CH_4/CO = 0.036$), whereas melamine-doped samples enhance CH_4 production. The highest CH_4/CO ratio (0.85) for melamine-derived catalysts is achieved with GDY-melamine-600. Crucially, the presence of sp-N atoms is the key differentiator, dramatically increasing the CH_4/CO ratio to 3.4:1 for eGDY-Click-700. XPS results (Figs. 7c and d) confirm the correlation between sp-N content and the observed breakthrough in CH_4 selectivity, identifying sp-N as the key active site. However, the reaction intermediate in this process has not been captured, impeding the understanding of the mechanism and the precise synthesis of metal-free catalysts. After four years of research, the fabrication of an intermediate-like molecule has been achieved, culminating in the synthesis of sp-N doped GDY *via* a pericyclic reaction. Compared to GDY doped with other N configurations, the designed sp-N GDY demonstrates significantly higher catalytic activity in the electroreduction of CO_2 towards CH_4 production. This is attributed to the unique electronic structure introduced by sp-N, which is more effective in stabilizing the intermediate. Thus, in addition to elucidating the site-defined doping process. As shown in Figs. 7f and g, the results can also be corroborated by *in situ* diffuse reflectance infrared Fourier transform spectroscopy (DRIFTS) to capture the intermediates. The peaks around 1520 and 1670 cm^{-1} can be attributed to CO_3^* (including bidentate and monodentate) and CO_2^* species for both

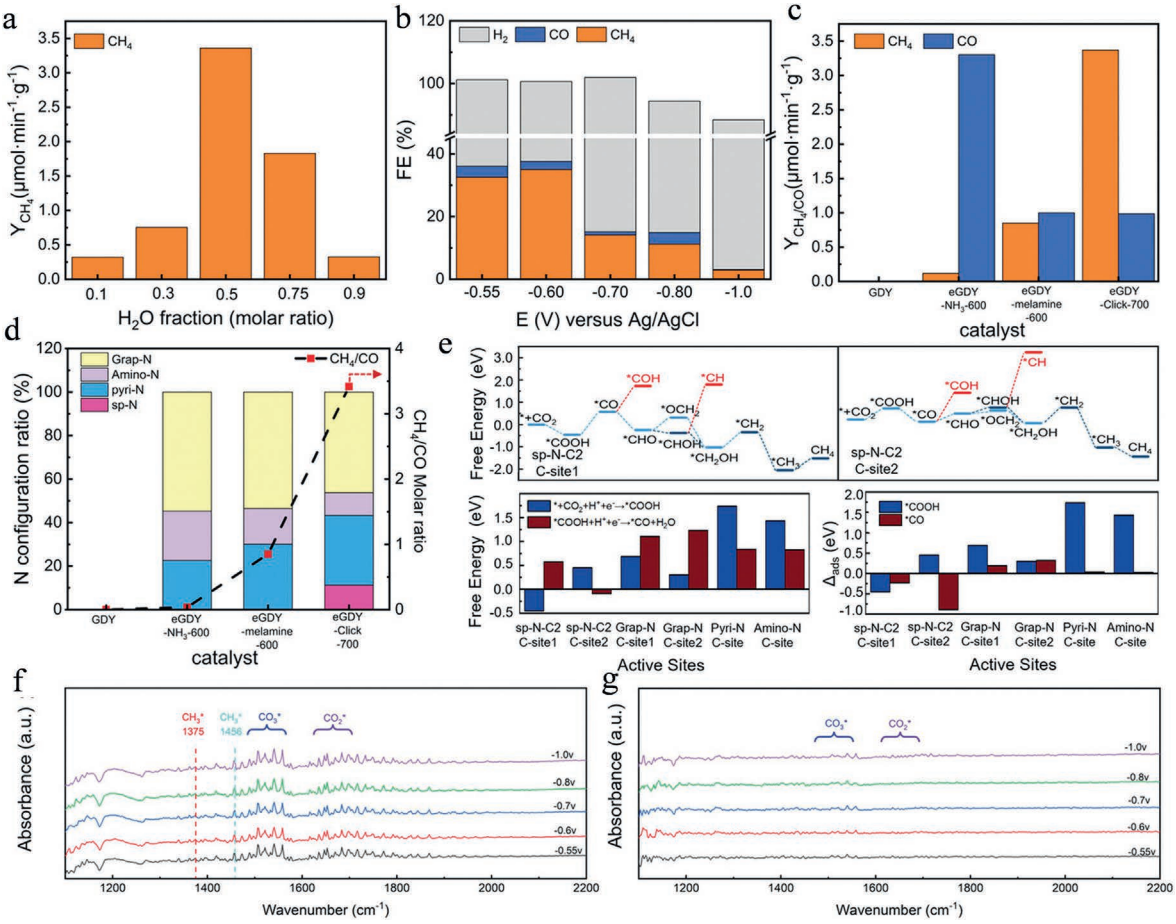


Fig. 7. (a) CH_4 productivity in electrolytes with varying water mole fractions. (b) Faradaic efficiency of products for eGDY-Click-700 at different potentials in EMIM-BF_4 electrolyte. (c) Yield rates of CH_4 and CO for various N-doped GDY samples. (d) The relationship between CH_4/CO molar ratios and N configurations in different N-doped carbon materials. (e) Energy profile for CH_4 formation from CO_2 induced by sp-N-C2 C-site 1 and sp-N-C2 C-site 2, including the free energy of *COOH and *CO at different active sites created by various N doping configurations, as well as the adsorption free energy of *COOH and *CO at these sites. (f, g) *In situ* DRIFTS spectra in the range of 1100–2200 cm^{-1} for detecting reaction intermediates in CO_2RR over eGDY-Click-700 and eGDY-NH_3-600. Reprinted with permission [141]. Copyright 2023, John Wiley and Sons.

eGDY-Click-700 and eGDY-NH_3-600, which serve as important intermediates for the subsequent production of C1 fuels. Additionally, distinct peaks at 1375 and 1456 cm^{-1}, corresponding to the CH_3* group, can be detected in eGDY-Click-700 during the CO_2RR process. This is recognized as a key intermediate in the CO_2-to-CH_4 conversion process. this work reveals the relationship between doping configuration and the products of CO_2 reduction. The reaction free energy profiles, the rate-limiting step, and the limiting potential for CO_2 electroreduction to CH_4 have been systematically examined. In Fig. 7e, it is evident that the energy required for the protonation of *CO to *CHO on sp-N is only −0.81 eV, indicating that this step does not serve as the main bottleneck of the process. Importantly, the adsorption free energies (ΔG_{ads}) for *COOH and *CO on sp-N are −0.45 eV and −0.23 eV, respectively. These values suggest that the intermediates are adsorbed with moderate strength, which is beneficial for the subsequent deep reduction of CO intermediates.

In previous research, besides N doping, Guo *et al.* employed computational methods to design a series of functionalized GDY-based materials and conducted a comprehensive investigation into the mechanisms of CO_2 adsorption. Their study elucidated the intrinsic relationships between functional groups, lithium atoms, and alkyne groups, and their performance in CO_2 capture. That work provided an effective and advanced alternative strategy for designing porous GDY-based materials for CO_2 adsorption and separation. Zhao *et al.* explored the catalytic activity of boron (B) or nitrogen (N) atom-doped GDY for the electrochemical reduction of CO_2 using density functional theory (DFT) computations [142]. Their findings indicated that the catalytic performance of these doped GDY materials was highly dependent on the dopant site. Specifically, doping sp-hybridized B and N atoms at the acetylenic sites of GDY exhibited superior catalytic performance for the conversion of CO_2 to CH_4 and particularly C_2H_4, with a low limiting potential of approximately −0.60 eV [15]. These results not only provide theoretical insights into the reduction pathways of CO_2 electrocatalytic reduction for the generation of C_1 and C_2 products but also pave a new path for designing highly efficient metal-free electrocatalysts for CO_2 conversion.

Furthermore, Few-layer oxidized GDY (FLGDYO) was utilized as the precursor, with melamine serving as the nitrogen source. Thermogravimetric-differential thermal analysis-mass spectrometry (TG-DTA-MS) demonstrated that during the calcination process, FLGDYO was reduced to few-layer GDY (FLGDY) through the release of CO_2^+ fragments. Concurrently, $NHCNH_2^+$ fragments released from melamine were adsorbed onto FLGDYO, followed by a pericyclic reaction that replaced sp-hybridized carbon atoms with nitrogen atoms. Transmission electron microscopy (TEM) and electron energy loss spectroscopy (EELS) mapping revealed a uniform distribution of carbon and nitrogen atoms across the ultrathin films, while the presence of sp-hybridized nitrogen was confirmed

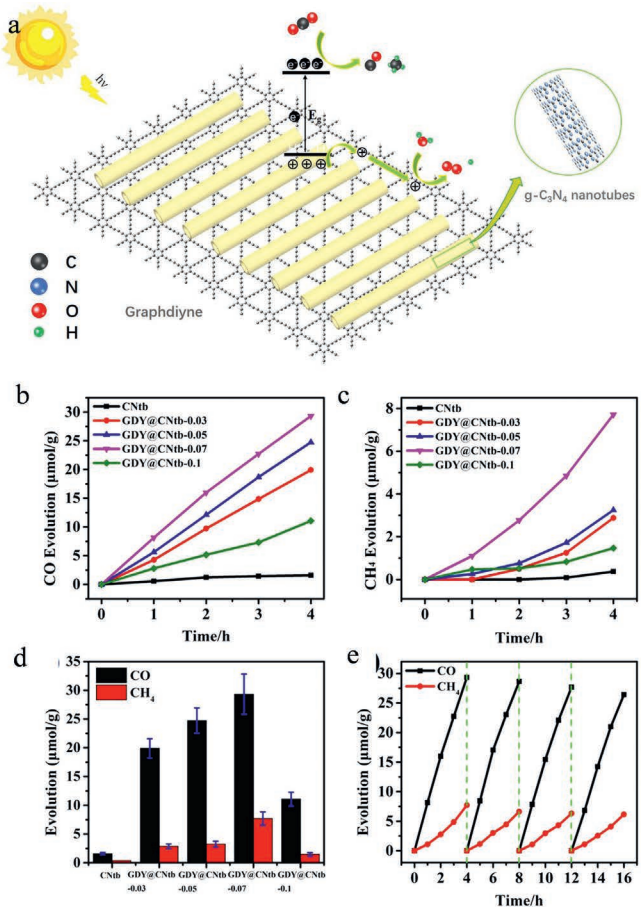


Fig. 8. (a) Proposed mechanism for the photocatalytic reduction of CO_2 over GDY@CNtb. (b) CO and (c) CH_4 evolution as a function of irradiation time for pure CNtb and GDY@CNtb composites with varying GDY to CNtb mass ratios. (d) Comparative analysis of CO and CH_4 yields across different samples after 4 h of illumination ($\lambda > 420$ nm). (e) Cyclic photocatalytic performance of GDY@CNtb-0.07 under prolonged illumination with a 420 nm. Reprinted with permission [144]. Copyright 2021, Elsevier.

by X-ray photoelectron spectroscopy (XPS) and X-ray absorption near edge structure (XANES) analysis. Additionally, the synthesis mechanism of sp-N-doped GDY was thoroughly investigated, leading to the identification of an intermediate-like molecule [141].

4.4. Photocatalytic CO_2RR by metal-free ACs GDY

In recent years, the two-dimensional nonmetallic organic semiconductor graphitic carbon nitride (g-C_3N_4) has garnered significant attention due to its favorable physical and chemical properties [118,143]. However, its poor conductivity and low charge separation efficiency pose challenges, which can be addressed by incorporating GDY. The excellent conductivity and carrier mobility of GDY present a novel approach for enhancing the photocatalytic reduction of CO_2. A simple self-assembly method was employed to prepare composites containing g-C_3N_4 nanotubes (GDY@CNtb), and the mechanisms underlying the photocatalytic CO_2 reduction on GDY@CNtb were explored. The introduction of GDY resulted in GDY@CNtb composites with significantly enhanced brightness in the visible spectrum and improved electrical conductivity. Consequently, the photocatalytic reduction of CO_2 was enhanced, and the composite's photocatalytic activity remained stable, demonstrating its robustness. When comparing the photocatalytic CO_2 reduction activity of GDY@CNtb with pure CNtb, the addition of GDY led to CO and CH_4 as the main products in Figs. 8a-d, the introduction of GDY significantly enhances the photocatalytic CO_2 reduction efficiency, with CO and CH_4 as the main products. Meanwhile, almost no H_2 is detected, likely due to its low yield. Additionally, the CO_2 reduction activity of GDY@CNtb increases with higher GDY content, reaching a maximum at a GDY to CNtb mass ratio of 0.07. As shown in Fig. 8e, after four cycles, the CO and CH_4 production continues to increase linearly with time, with no significant decline observed. Significantly improving the photocatalytic efficiency for CO_2 reduction [144]. GDY@CNtb exhibited desirable photocatalytic activity. Furthermore, through simulation calculations, a comparison of the performance of different metals anchored on GDY for CO_2RR reduction was obtained. This provides a meaningful theoretical basis for subsequent photoelectrocatalytic CO_2 reduction.

5. Conclusions and prospects

5.1. Conclusion

GDY holds significant potential for applications in environmental, energy, and catalytic fields. Extensive research has been conducted on the synthesis of GDY and its various properties, including electronic, energy storage, and catalytic characteristics. However, there remains substantial potential for further development and application. Notable progress has been achieved in SACs on GDY for reactions especially CO_2RR. SACs on GDY are particularly promising due to their maximum atomic utilization and exceptional catalytic performance, leading to significant advancements in multiphase and catalytic processes. The unique planar structure of GDY allows for the exposure of active sites during catalysis, effectively enhancing atom utilization. GDY demonstrates significant advantages over traditional two-dimensional carbon materials such as graphene and g-C_3N_4 in stabilizing SACs. Its unique porous architecture and highly π-conjugated structure provide abundant and robust anchoring sites, ensuring high dispersion and stability of single atoms. GDY derivatives offer a means to modulate the interaction between metal atoms and the support to achieve optimal electrocatalytic performance. Metal-doped GDY more effectively facilitates photo/electrocatalytic carbon dioxide reduction. Specifically, GDY doped with copper (Cu) and iron (Fe) exhibits excellent Faradaic efficiency and promotes the formation of C_2 products. For non-metallic doped GDY, nitrogen (N) doping more readily facilitates photo/electrocatalytic CO_2 reduction. Structurally, non-metallic elements are more uniformly distributed within GDY, and the lone pair electrons of non-metals are more readily available to provide electrons for CO_2 reduction. However, in terms of photo/electrocatalytic performance, metal doping exhibits more advantageous properties. This is due to the larger specific surface area of metals, which allows metal centers to adsorb CO_2 and reduce the band gap more easily. Furthermore, attention should be directed towards introducing heteroatoms coordinated with single-atom sites to create new active sites with potentially diverse catalytic effects. While theoretical calculations have elucidated the adsorption behavior of reaction intermediates on active sites, the design of active site configurations requires further exploration. Therefore, developing methods for the large-scale, cost-effective production of GDY and its derivatives is essential. It is anticipated that GDY and its derivatives will play a pivotal role in the future of SACs.

5.2. Challenges and perspective

Despite the promising properties of GDY as a support for (SACs, several critical challenges must be addressed to facilitate its practical application.

5.2.1. Challenges in large-scale synthesis and material quality

Firstly, the large-scale production of high-quality GDY remains a significant bottleneck. The current synthesis procedures are complex, often requiring high-purity precursors, stringent reaction conditions, and sophisticated equipment. These factors collectively contribute to high production costs and limit scalability. Moreover, the reproducibility of GDY synthesis is often compromised by batch-to-batch variations, which can affect the uniformity of the material's structure and properties. To overcome these issues, it is essential to conduct comprehensive cost analyses and develop more economical, scalable, and robust synthesis routes. Innovations such as continuous-flow synthesis, green chemistry approaches, and the use of more readily available raw materials could be explored to facilitate industrial adoption.

5.2.2. Uniformity and control of single-atom loading

Achieving reproducible and uniform SAC loading on GDY is another major challenge. Variations in the density and distribution of anchoring sites can lead to inconsistencies in catalytic performance across different batches. This is particularly problematic for single-atom doped GDY, where the uneven distribution of metal single atoms complicates mechanistic investigations and hinders the rational design of catalysts. Standardized synthesis protocols, advanced *in situ* characterization techniques, and atomic-level control over anchoring site formation are urgently needed. Furthermore, precise regulation of the coordination environment around single atoms remains difficult, limiting the ability to systematically study structure–activity relationships and optimize catalytic performance.

5.2.3. Integration into industrial systems

The integration of SAC-GDY catalysts into industrial reactors, such as flow cells for electrochemical CO_2RR, presents additional hurdles. Material processability, mechanical stability, and compatibility with existing reactor configurations are critical factors that must be addressed. For example, the morphology, thickness, and mechanical strength of GDY-based materials can influence their performance and durability under industrially relevant conditions. Developing methods to fabricate GDY materials with tailored physical properties and ensuring their seamless integration into devices are key steps toward practical deployment.

5.2.4. Stability and durability under operating conditions

The stability of single-atom doped GDY catalysts during operation is a crucial concern. Additionally, under continuous electrochemical operation, single atoms may migrate or aggregate, resulting in performance degradation over time. Strategies such as engineering robust anchoring sites, introducing protective surface architectures, and optimizing the electronic structure of GDY are necessary to enhance the long-term stability and durability of these catalysts.

5.2.5. Electrochemical performance and selectivity

Single-atom doped GDY catalysts also face challenges related to electrochemical performance. High overpotentials can limit energy efficiency, while selectivity issues arise due to competing side reactions, such as the hydrogen evolution reaction (HER), which can reduce the yield of desired products in processes like CO_2 reduction. Rational design of the coordination environment, such as introducing heteroatom dopants or modulating the electronic structure of GDY, can help lower overpotentials and improve selectivity. Continued research into these strategies is essential for advancing the practical application of SAC-GDY in electrocatalysis.

5.2.6. Limitations and opportunities for non-metal doping

Non-metal-doped GDY offers the advantage of more uniform heteroatom introduction; however, its photocatalytic CO_2 reduction performance is generally lower than that of metal-doped GDY, particularly in the production of multi-carbon (C_2) products. The variety of non-metal single atoms available for doping is limited, and only a few non-metal atoms can provide the necessary lone pair electrons for effective catalysis. Expanding the diversity of non-metal dopants and exploring multi-element doping strategies could enhance the catalytic efficiency and broaden the application scope of non-metal-doped GDY.

5.2.7. Cost, environmental impact, and raw material availability

Some synthesis methods for GDY and its derivatives require high-purity precursors, specific metal sources, or specialized solvents, which increase overall costs and may pose environmental concerns. High-temperature or special-atmosphere treatments further contribute to energy consumption and environmental impact. Therefore, developing low-energy, environmentally friendly, and cost-effective synthesis processes is an important direction for future research.

In summary, combining the advantages of both metal and non-metal doping in GDY presents a promising strategy for overcoming current limitations. For instance, introducing electron-rich non-metal single atoms into the structural monomer, followed by complexation with various metals and subsequent GDY synthesis, can yield stable coordination structures. This approach enables uniform distribution of metal single atoms and enhances catalytic activity. Structurally, such hybrid materials can leverage the synergistic effects of metals and non-metals, achieving both diversity in catalytic applications and improved structural features. This strategy not only addresses the shortcomings of individual doping approaches but also opens up new avenues for the rational design of high-performance catalysts for CO_2 reduction and other important reactions.

CRediT authorship contribution statement

Fangzhou Yang: Writing – review & editing, Writing – original draft. **Yangmin Ma:** Writing – review & editing, Supervision. **Siyue Ma:** Investigation, Conceptualization. **Linli Xu:** Writing – review & editing, Supervision, Resources, Investigation.

Declaration of competing interest

The authors declare that they have no known competing financial interests or personal relationships that could have appeared to influence the work reported in this paper.

Acknowledgments

Y. Ma thanks the National Natural Science Foundation of China (No. 22178205), L. Xu thanks The Hong Kong Research Grants Council (No. PolyU 25301524), The Hong Kong Research Grants Council, Young Collaborative Research Grant (No. C5001-24), Guangdong Provincial Natural Science Foundation-General Project (No. 2024A1515010422).

References

[1] Y. Du, X. Zheng, Y. Xue, Y. Li, Chem. Res. Chin. Univ. 38 (2022) 1380–1386.
[2] Z. Feng, Y. Tang, Y. Ma, et al., Appl. Surf. Sci. 538 (2021) 148145.
[3] C. He, H. Yang, L. Fu, Chin. Chem. Lett. 34 (2023) 107581.
[4] M. Khalil, G.T.M. Kadja, F.A.A. Nugroho, et al., Renew. Sustain. Energy Rev. 206 (2024) 114869.
[5] X. Chen, A. Xu, D. Wei, et al., Chin. Chem. Lett. 36 (2025) 110175.
[6] C. Huang, J. Liu, H.H. Huang, X. Xu, Z. Ke, Chin. Chem. Lett. 33 (2022) 262–265.

[7] Q. Huang, R. Wang, X. Li, et al., Chin. Chem. Lett. 34 (2023) 108517.
[8] H. Li, C. Gao, G. Yang, et al., Chin. Chem. Lett. 36 (9) (2025) 110547.
[9] L. Jiang, M. Zhao, Q. Yu, RSC Adv. 14 (2024) 27365–27371.
[10] P. Joby, Y. Manojkumar, A. Rajendran, R.V. Solomon, Front. Chem. Sci. Eng. 18 (2024) 132.
[11] Y. Sun, X. Liu, M. Zhu, et al., DeCarbon 2 (2023) 100018.
[12] S. Zhou, S. Cao, S. Wei, et al., Appl. Mater. Today 25 (2021) 101245.
[13] Z. Zheng, F. He, Y. Xue, Y. Li, Chem. Res. Chin. Univ. 38 (2021) 92–98.
[14] M. Zhao, L. Jiang, Q. Yu, Catal. Sci. Technol. 13 (2023) 5154–5174.
[15] J. Zhao, Z. Chen, J. Zhao, J. Mater. Chem. A 7 (2019) 4026–4035.
[16] J. Zhang, F. Wang, G. Qi, et al., Adv. Funct. Mater. 31 (2021) 2101423.
[17] M. Sun, H.H. Wong, T. Wu, A.W. Dougherty, B. Huang, Adv. Energy Mater. 12 (2022) 2103781.
[18] C. Yang, Y. Wang, J. Yu, S. Cao, ACS Appl. Energy Mater. 4 (2021) 8734–8738.
[19] C. Zhang, Y. Xue, X. Zheng, L. Qi, Y. Li, Mater. Today 66 (2023) 72–83.
[20] S. Yu, J. Chen, C. Chen, et al., Coordin. Chem. Rev. 482 (2023) 215082.
[21] J. Yu, Y. Yang, Y. Li, C. Cao, W. Song, Nano Res. 17 (2023) 2223–2233.
[22] H. Yu, Y. Xue, L. Hui, et al., Natl. Sci. Rev. 8 (2021) 213.
[23] J. Wang, J. Zhao, S. Wang, J. Yu, N. Li, Chin. Chem. Lett. 37 (2026) 111859.
[24] F. Xu, K. Meng, B. Zhu, et al., Environ. Sci. Ecotechnol. 29 (2019) 1904256.
[25] W. Xie, S. Zhang, Y. Ni, et al., Adv. Energy Sustain. Res. 2 (2021) 2100037.
[26] K. Azizi, S.M. Vaez Allaei, A. Fathizadeh, et al., Sci. Rep. 11 (2021) 16325.
[27] S. Chen, X. Zheng, Y. Gao, et al., Precis. Chem. 2 (2024) 355–375.
[28] X. Chen, F. He, W. Fang, et al., ACS Cent. Sci. 6 (2020) 779–786.
[29] X. Chen, Z.Z. Lin, M. Ju, L.X. Guo, Appl. Surface Sci. 479 (2019) 685–692.
[30] C. Song, G. Li, Chem. Res. Chin. Univ. 37 (2021) 1224–1241.
[31] T. Zhang, Y.J. Wang, L.M. Yu, et al., New Carbon Mater. 37 (2022) 1089–1113.
[32] J. Li, X. Gao, X. Jiang, et al., ACS Catal. 7 (2017) 5209–5213.
[33] J. Cui, J. Liu, C. Wang, et al., Electrochimica Acta 334 (2020) 135577.
[34] H. Dai, T. Song, X. Yue, et al., Chin. J. Catal. 64 (2024) 123–132.
[35] H. Ding, J. He, L. Ding, H. Tian, DeCarbon 4 (2024) 100048.
[36] S. Feng, C. Zhao, T. Zhao, Y. Tian, L. Yan, Colloids Surf. A: Physicochem. Eng. Aspects 655 (2022) 130229.
[37] X. Fu, X. Zhao, T.B. Lu, M. Yuan, M. Wang, Angew. Chem. Int. Ed. 62 (2023) e202219242.
[38] T. He, L. Zhang, G. Kour, A. Du, CO_2 Utilization 37 (2020) 272–277.
[39] X. Hu, N.Q. Su, W.H. Fang, J. Phys. Chem. C 127 (2023) 11026–11039.
[40] R. Huang, Z. Kou, R.D. Rodriguez, et al., ACS Appl. Nano Mater. 6 (2023) 7395–7403.
[41] B. Li, C. Lai, M. Zhang, et al., Adv. Energy Mater. 10 (2020) 2000177.
[42] H. Li, J.H. Lim, Y. Lv, et al., Chem. Rev. 123 (2023) 4795–4854.
[43] J. Li, C. Wan, C. Wang, H. Zhang, X. Chen, Chem. Res. Chin. Univ. 36 (2020) 622–630.
[44] S. Liang, H. Deng, Z. Zhou, W.Y. Wong, EcoMat 5 (2022) e12297.
[45] M. Cui, T. Hu, L. Chen, et al., Wang, ChemElectroChem 7 (2020) 4843–4852.
[46] T. Jitwatanasirikul, T. Roongcharoen, P. Sikam, et al., Adv. Mater. Interfaces 10 (2023) 2201904.
[47] X. Li, X. Cui, L. Zhang, J. Du, ACS Appl. Nano Mater. 6 (2023) 20493–20522.
[48] C. Pan, C. Wang, Y. Fang, et al., Environ. Sci.: Nano 8 (2021) 1863–1885.
[49] M. Ren, X. Guo, S. Zhang, S. Huang, Adv. Funct. Mater. 33 (2023) 2213543.
[50] P. Shandilya, P. Mandyal, V. Kumar, M. Sillanpää, Sep. Purif. Technol. 281 (2022) 119825.
[51] J.J. Wang, H.J. Wang, C. Zhang, et al., 2D Materials 8 (2021) 044008.
[52] L. Wang, Z. Liu, J. Zhang, Nanoscale 14 (2022) 13473–13489.
[53] M. Wang, J. Pu, Y. Hu, et al., Adv. Funct. Mater. 34 (2023) 2308601.
[54] B. Wu, M. Li, S. Xiao, et al., Nanoscale 9 (2017) 11939–11943.
[55] C. Xie, N. Wang, X. Li, G. Xu, C. Huang, Chem. Eur. J. 26 (2019) 569–583.
[56] J. Yang, B. Gao, W. Liu, J. Du, Q. Xu, ChemPhysChem 24 (2023) e202200793.
[57] P. Wu, P. Du, H. Zhang, C. Cai, Phys. Chem. Chem. Phys. 16 (2014) 5640–5648.
[58] Z. Zhou, J. Wang, M. Reheimujiang, Z. Jin, J. Mater. Sci. Technol. 213 (2025) 241–251.
[59] Z. Liu, Y. Ding, X. Li, et al., Surf. Sci. 724 (2022) 122133.
[60] Y. Gao, Z. Cai, X. Wu, et al., ACS Catal. 8 (2018) 10364–10374.
[61] H. Yu, Y. Xue, B. Huang, et al., iScience 11 (2019) 31–41.
[62] J. Li, L. Zhong, L. Tong, et al., Adv. Funct. Mater. 29 (2019) 1905423.
[63] M. Li, Q. Lv, W. Si, Z. Hou, C. Huang, Angew. Chem. Int. Ed. 61 (2022) e202208238.
[64] J. Yu, C. Cao, H. Jin, et al., Natl. Sci. Rev. 9 (2022) nwac018.
[65] L. Hui, Y. Xue, H. Yu, et al., J. Am. Chem. Soc. 141 (2019) 10677–10683.
[66] H. Zou, W. Rong, S. Wei, Y. Ji, L. Duan, Proc. Natl. Acad. Sci. U. S. A. 117 (2020) 29462–29468.
[67] Q. Lv, W. Si, Z. Yang, et al., ACS Appl. Mater. Interfaces 9 (2017) 29744–29752.
[68] M. Liu, Y. Pang, B. Zhang, et al., Nature 537 (2016) 382–386.
[69] S. Zhang, H. Du, J. He, et al., ACS Appl. Mater. Interfaces 8 (2016) 8467–8473.
[70] L. Hao, S. Zhang, R. Liu, et al., Adv. Mater. 27 (2015) 3190–3195.
[71] Y. Zhao, N. Yang, H. Yao, Liu, et al., J. Am. Chem. Soc. 141 (2019) 7240–7244.
[72] H. Liu, H. Zou, M. Wang, et al., Small 18 (2022) e2203442.
[73] I. Muhammad, U. Younis, W. Wu, et al., J. Power Sources 480 (2020) 228876.
[74] X. Shen, J. He, K. Wang, et al., ChemSusChem 12 (2019) 1342–1348.
[75] X. Kan, Y. Ban, C. Wu, et al., ACS Appl. Mater. Interfaces 10 (2017) 53–58.
[76] Y. Wang, J. An, L. Qi, et al., J. Am. Chem. Soc. 145 (2023) 864–872.
[77] N. Wang, J. He, Z. Tu, et al., Angew. Chem. Int. Ed. 56 (2017) 10740–10745.
[78] Z. Jin, H. Gong, Adv. Mater. Interfaces 8 (2021) 2100630.
[79] J. Cheng, S. Wan, S. Cao, Angew. Chem. Int. Ed. 62 (2023) e202310476.
[80] X. Ma, H. Cheng, Appl. Catal. B: Environ. 339 (2023) 123101.
[81] R. Matsuoka, R. Toyoda, R. Shiotsuki, et al., ACS Appl. Mater. Interfaces 11 (2019) 2730–2733.
[82] X. Wang, Z. Fu, L. Zheng, et al., Chem. Mater. 32 (2020) 9107–9114.
[83] Q. Liao, K. Sun, J. Wang, DeCarbon 1 (2023) 100001.
[84] T. Liu, T. Xu, T. Li, Y. Jing, J. Am. Chem. Soc. 146 (2024) 24133–24140.
[85] T. Lu, H. Wang, Nano Res. 15 (2022) 9764–9778.
[86] X. Lu, Y. Han, T. Lu, Acta Phys. Chim. Sinica 34 (2018) 1014–1028.
[87] Q. Liu, J. Lin, H. Cheng, L. Wei, F. Wang, Angew. Chem. Int. Ed. 62 (2023) e202218720.
[88] R. Xu, X.S. Wang, H. Zhao, et al., Catal. Sci. Technol. 8 (2018) 2224–2230.
[89] L. Ye, Y. Deng, L. Wang, H. Xie, F. Su, ChemSusChem 12 (2019) 3671–3701.
[90] Z. Feng, Y. Tang, Y. Ma, et al., Int. J. Hydrogen Energy 46 (2021) 5378–5389.
[91] Y. Dong, S. Semin, Y. Feng, J. Xu, T. Rasing, Chin. Chem. Lett. 32 (2021) 525–528.
[92] W. Li, Y. Zhang, Y. Wang, et al., Appl. Catal. B: Environ. 340 (2024) 123267.
[93] H. Li, C. Gao, G. Yang, et al., Chin. Chem. Lett. 36 (2025) 110547.
[94] M. Khalid, B.S. De, S. Shahgaldi, DeCarbon 6 (2024) 100074.
[95] J. Lian, D. Li, Y. Ma, et al., Chin. Chem. Lett. 36 (11) (2025) 111394.
[96] B. Chen, Y.F. Jiang, H. Xiao, J. Li, ACS Catal. 14 (2024) 10510–10518.
[97] S. Cao, Y. Wang, B. Zhu, G. Xie, J. Yu, J.R. Gong, J. Mater. Chem. A 8 (2020) 7671–7676.
[98] A. Borchers, T. Pieler, Genes 1 (2010) 413–426.
[99] X. Chen, X. Zheng, C. Zhang, et al., Nano Energy 114 (2023) 108622.
[100] G. Liu, Y. Zhou, Q. Yan, Y. Doekhi-Bennani, Chin. Chem. Lett. 32 (2021) 2819–2822.
[101] X. Liu, C. Wang, J. Meng, et al., Chin. Chem. Lett. 34 (2023) 108745.
[102] Y. Ma, H. Qu, W. Wang, et al., Chin. Chem. Lett. 35 (2024) 108352.
[103] Y. Man, J. Zhao, S. Liu, Q. Pan, Y. Zhao, ACS Appl. Mater. Interfaces 37 (2021) 1213–1223.
[104] H. Zhang, C. He, S. Han, et al., Chin. Chem. Lett. 33 (2022) 3641–3649.
[105] I. Muhammad, S. Ahmed, H. Cao, et al., Mater. Today Chem. 34 (2023) 101756.
[106] Y. Ni, L. Miao, J. Wang, et al., Phys. Chem. Chem. Phys. 22 (2020) 1181–1186.
[107] K. Su, G.X. Dong, W. Zhang, et al., ACS Appl. Mater. Interfaces 12 (2020) 50464–50471.
[108] C. Sun, S. Huang, M. Huang, et al., Adv. Rev. 50 (2021) 10867–10879.
[109] Q. Pan, X. Chen, H. Liu, et al., Mater. Chem. Front. 5 (2021) 4596–4603.
[110] P.K. Prajapati, A. Malik, N. Nandal, et al., Appl. Surface Sci. 588 (2022) 152912.
[111] S. Rana, A. Kumar, P. Dhiman, et al., Fuel 356 (2024) 129630.
[112] A. Moreno-Zuria, J.G. Rivera, A.U. Chávez-Ramírez, M. Mohamedi, DeCarbon 4 (2024) 100046.
[113] J. Zhang, Y. Wang, H. Wang, D. Zhong, T. Lu, Chin. Chem. Lett. 33 (2022) 2065–2068.
[114] M. Zhang, T. Xu, R. Yin, et al., Chin. Chem. Lett. 37 (2026) 110665.
[115] C. Zuo, L. Tan, H. Dong, et al., DeCarbon 2 (2023) 100020.
[116] H. Zhang, N.G. Park, DeCarbon 3 (2024) 100025.
[117] S. Rana, A. Kumar, T.T. Wang, et al., New Carbon Mater. 39 (2024) 458–482.
[118] Y. Ren, Y. Dong, Y. Feng, J. Xu, Catalysts 8 (2018) 590.
[119] P. Rezaee, H.R. Naeij, Sci. Rep. 10 (2020) 13549.
[120] M.J. Saadh, W.M. Bravo Morocho, Y. Ajaj, et al., Sustain. Chem. Pharm. 38 (2024) 101487.
[121] G. Shi, C. Yu, Z. Fan, J. Li, M. Yuan, ACS Appl. Mater. Interfaces 11 (2019) 2662–2669.
[122] M. Tahir, B. Tahir, N.A.S. Amin, Appl. Catal. B: Environ. 204 (2017) 548–560.
[123] D. Tan, J. Zhang, J. Shi, et al., ACS Appl. Mater. Interfaces 10 (2018) 24516–24522.
[124] M. Sun, B. Huang, Adv. Energy Mater. 13 (2023) 2301948.
[125] S. Cao, Y. Xue, X. Chen, et al., Mater. Chem. Front. 7 (2023) 2620–2627.
[126] H. Dai, H. Zou, T. Song, et al., Inorg. Chem. Front. 10 (2023) 2189–2196.
[127] W. Rong, H. Zou, W. Zang, et al., Angew. Chem. Int. Ed. 60 (2021) 466–472.
[128] D.H. Lim, J.H. Jo, D.Y. Shin, et al., Nanoscale 6 (2014) 5087–5092.
[129] X. Liu, Z. Wang, Y. Tian, J. Zhao, J. Phys. Chem. C 124 (2020) 3722–3730.
[130] A.J. Shih, N. Arulmozhi, M.T.M. Koper, ACS Catal. 11 (2021) 10892–10901.
[131] Z. Zheng, Z. Wang, Y. Xue, F. He, Y. Li, ACS Mater. Au 1 (2021) 107–115.
[132] Z. Wu, J. Liu, B. Mu, et al., Appl. Surf. Sci. 648 (2024) 159027.
[133] L. Fan, X. Yang, Q. Xiao, X. Guo, Z. Jin, Sep. Purif. Technol. 354 (2025) 128738.
[134] R.K. de_Richter, T. Ming, S. Caillol, Renew. Sustain. Energy Rev. 19 (2013) 82–106.
[135] Y. He, Y. Zhao, X. Wang, et al., Angew. Chem. Int. Ed. 62 (2023) e202307160.
[136] J. Li, L. Zhu, C.H. Tung, L.Z. Wu, Angew. Chem. Int. Ed. 62 (2023) e202301384.
[137] Q. Li, B. Guo, J. Yu, et al., J. Am. Chem. Soc. 133 (2011) 10878–10884.
[138] T. Li, N. Tsubaki, Z. Jin, J. Mater. Sci. Technol. 169 (2024) 82–104.
[139] G. Hu, J. He, Y. Li, Chem. Res. Chin. Univ. 37 (2021) 1195–1212.
[140] S. Shyamal, S.K. Dutta, N. Pradhan, J. Phys. Chem. Lett. 10 (2019) 7965–7969.
[141] B. Liu, S. Zhan, J. Du, et al., Adv. Mater. 35 (2023) e2206450.
[142] Y. Dang, W. Guo, L. Zhao, H. Zhu, ACS Appl. Mater. Interfaces 9 (2017) 30002–30013.
[143] S. Sambyal, R. Sharma, P. Mandyal, et al., J. Environ. Chem. Eng. 11 (2023) 109517.
[144] C. Sun, Y. Liu, Z. Wang, et al., J. Alloys Compd. 868 (2021) 159045.